

# Cosmological Implications and Stability of $f(\mathbb{Q}, \mathbb{T})$ Gravity with Pilgrim Dark Energy Model

M. Sharif<sup>1,2</sup> \* and Iqra Ibrar<sup>1</sup> †

<sup>1</sup> Department of Mathematics and Statistics, The University of Lahore,  
1-KM Defence Road Lahore-54000, Pakistan.

<sup>2</sup> Research Center of Astrophysics and Cosmology, Khazar University,  
Baku, AZ1096, 41 Mehseti Street, Azerbaijan.

## Abstract

This manuscript endeavors to construct a pilgrim dark energy framework within the  $f(\mathbb{Q}, \mathbb{T})$  gravity theory, employing a correspondence approach aligned with a non-interacting model that incorporates pressureless matter alongside a power-law scale factor. Here  $\mathbb{Q}$  and  $\mathbb{T}$  represent the non-metricity and trace of the energy-momentum tensor, respectively. This extended modified gravity framework accurately replicates various epochs in the cosmological history. The  $f(\mathbb{Q}, \mathbb{T})$  gravity models are utilized to derive the equation of state parameter, phase planes and squared speed of sound. The analysis reveals that the reconstructed model exhibits an increasing or decreasing trend with the pilgrim dark energy parameter. The equation of state parameter characterizes the phantom regime, while the squared speed of sound parameter provides a stable framework for examining the ongoing cosmic evolution. The  $\omega_{DE} - \omega'_{DE}$  plane trajectories reveal the freezing region, while the  $r - s$  phase plane shows the Chaplygin gas model. It is important to highlight that our findings align with the most recent observational data.

---

\*msharif.math@pu.edu.pk

†iqraibrar26@gmail.com

**Keywords:** Cosmic diagnostic parameters; Pilgrim dark energy model;  $f(\mathbb{Q}, \mathbb{T})$  gravity.

**PACS:** 64.30.+t; 95.36.+x; 04.50.kd.

## 1 Introduction

The general theory of relativity (GR) is a foundational pillar of physics, revolutionizing our comprehension of gravity and the fabric of spacetime. It is validated through comprehensive studies and empirical evidences. However, this theory depends on the geometric patterns found within Riemannian metric space. Weyl [1] devised an expansive geometric framework that surpasses Riemannian space, offering a complete description of gravitational field and matter. He focused on unifying gravitational and electromagnetic forces, rather than attempting to combine all fundamental forces. The Levi-Civita (LC) connection serves as a cornerstone in Riemannian geometry, enabling the comparison of vectors based on their lengths. In contrast, Weyl introduced a groundbreaking concept that disregards vector magnitudes during parallel transport. To address the absence of length information, he introduced an additional component known as the length connection. Unlike the LC connection, which preserves vector direction, the length connection adjusts the conformal factor without affecting the direction of transport. Non-Riemannian (NR) geometries extend the principles of Riemannian geometry to provide a more nuanced understanding of spacetime curvature. These geometrical frameworks incorporate elements such as torsion and the non-metricity tensor ( $\mathbb{Q}$ ). According to Weyl's theory, the existence of  $\mathbb{Q}$  arises from the metric tensor possessing a non-zero covariant derivative. [2].

The concept of  $\mathbb{Q}$  within NR geometries offers an alternative cosmological framework that eliminates the need for dark energy (DE). In NR gravity models, the metric, coframe and full connection serve as gauge potentials [3]. The associated field strengths include non-metricity tensor  $\mathbb{Q}_{\alpha\beta}$ , torsion scalar  $T$ , and curvature tensor  $\mathbb{R}_{\alpha\beta}$ . The NR gravity models are primarily investigated due to the absence of experimental findings regarding  $\mathbb{Q}$  and torsion. The classification of spacetimes and associated concepts is provided in Table 1.

In STG, gravitational interactions are governed by the non-metricity scalar, as opposed to the Ricci scalar  $\mathbb{R}$  in general relativity or the torsion scalar  $T$  in teleparallel gravity. A notable strength of using  $\mathbb{Q}$  lies in its

second-order field equations, which avoid the higher-order derivatives common in curvature-based models like  $f(\mathbb{R}, \mathbb{T})$ . This leads to simpler, more stable cosmological formulations while still allowing for modified dynamics. Additionally,  $f(\mathbb{Q}, \mathbb{T})$  models can reproduce cosmological observations such as large-scale structure and redshift space distortions without relying on DE, presenting a viable alternative to the  $\Lambda$ CDM paradigm. Non-metricity also offers a cleaner geometric interpretation by separating gravitational effects from curvature and torsion. In STG and its extensions, spacetime is flat and torsionless, with gravity emerging from variations in length and angle under parallel transport. This provides a fully covariant and frame-independent formulation unlike  $f(T)$  theories, which suffer from frame dependence due to their reliance on the tetrad formalism. Moreover, introducing the trace of the EMT in  $f(\mathbb{Q}, \mathbb{T})$  gravity enables non-minimal coupling between matter and geometry. This coupling introduces new degrees of freedom, offering greater flexibility for modeling late time cosmic acceleration and the dynamics of DE without exotic fields. From a cosmological standpoint, recent studies [4] have shown that  $f(\mathbb{Q}, \mathbb{T})$  theories can successfully reproduce accelerated expansion, phantom crossings, and even inflation, often outperforming  $f(\mathbb{R})$  and  $f(T)$  models in observational compatibility.

Scholars are increasingly attracted towards the study of NR geometry, especially  $f(\mathbb{Q})$  theory, due to its potential to reshape theoretical frameworks, its agreement with observational evidence and its crucial role in advancing cosmological theories [5]. Barros et al. [6] examined the cosmic properties by utilizing redshift space distortion data within the framework of non-metric gravity theory. The modified theory [7] can clarify the cosmic bounce scenario. Sharif and Ajmal [8] examined the cosmological features of GGDE  $f(\mathbb{Q})$  gravity, while Sharif et al. [9] investigated the phenomenon of the cyclic universe within NR geometry.

Modified STG incorporates the trace of the EMT into the action integral, resulting in the  $f(\mathbb{Q}, \mathbb{T})$  theory. The inclusion of  $\mathbb{T}$  allows the gravitational field equations to directly couple to the matter content of the universe, introducing additional degrees of freedom. This coupling enables the model to reflect how matter distribution influences spacetime geometry, potentially explaining phenomena such as cosmic acceleration without requiring exotic DE. Specifically,  $\mathbb{T}$  encapsulates matter density and pressure, providing a mechanism by which the universe's energy distribution affects gravitational interactions. This approach expands the scope of potential cosmological solutions while offering a unified framework to address both early time inflation

Table 1: Categorization of spacetimes

Relations	Spacetimes	physical representations
$Q_{\mu\nu} = 0, T = 0, R_{\mu\nu} = 0$	Minkowski	Special Relativity
$Q_{\mu\nu} = 0, T = 0, R_{\mu\nu} \neq 0$	Riemannian	General Relativity
$Q_{\mu\nu} = 0, T \neq 0, R_{\mu\nu} = 0$	Weitzenböck	Teleparallel Gravity
$Q_{\mu\nu} \neq 0, T = 0, R_{\mu\nu} = 0$		Symmetric Teleparallel
$Q_{\mu\nu} \neq 0, T = 0, R_{\mu\nu} \neq 0$	Riemann-Weyl	Einstein-Weyl
$Q_{\mu\nu} = 0, T \neq 0, R_{\mu\nu} \neq 0$	Riemann-Cartan	Einstein-Cartan
$Q_{\mu\nu} \neq 0, T \neq 0, R_{\mu\nu} \neq 0$	Non-Riemannian	Einstein-Cartan-Weyl

and the late time acceleration of the cosmos. Unlike many modified gravity theories that rely on extra fields or fine tuning,  $f(Q, T)$  extends GR naturally by modifying the spacetime geometry itself, offering flexibility in fitting observational data and generating new predictions for large scale cosmic behavior. With its second-order field equations, this theory also simplifies calculations, enhancing its practicality for theoretical studies. While promising,  $f(Q, T)$  gravity is still emerging and further studies are essential to fully understand its implications.

Recent research has begun to explore its cosmological applications, demonstrating its potential to address fundamental questions about the nature of DE and the universe accelerated expansion. Pati et al. [11] analyzed the evolutionary pattern of cosmological parameters, observing a marginal change in the behavior of the equation of state parameter (EoS). Narawade et al. [12] studied the dynamic behavior of an accelerating cosmological paradigm in this gravity to confirm its stability. Venkatesha et al. [13] explored the existence of traversable wormhole solutions within this extended theoretical framework. Gadbail et al. [14] examined the evolution of the universe within this modified theory to gain insights into accelerated expansion and other phenomena. Bourakadi et al. [15] examined the impact of  $f(Q, T)$  gravity on the formation of primordial black holes. Their research suggests that this theoretical framework could significantly influence the dynamics of inflation. Shekh [16] focused on late-time cosmic acceleration within the same framework, proposed a new scale factor and conducted a statefinder analysis. Gul et al. [17] explored the feasibility and structural integrity of compact stellar objects by considering various factors within this theory. Khurana et

al. [18] explored a higher order time-dependent function of the deceleration parameter with restrictions from observations in the same theory.

Pati et al. [19] explored little rip, big rip, and pseudo rip cosmologies within extended STG using the form  $f(Q, T) = aQ^m + bT$ , deriving field equations, energy conditions and cosmographic parameters in terms of non-metricity. Agrawal et al. [20] present a cosmological model based on a generalized gravitational action, constraining its parameters with current Hubble, Pantheon+ and Baryon Acoustic Oscillations data, which reveals a universe evolving from early deceleration to accelerating expansion and favoring a phantom field dominated phase. Narawade et al. [21] proposed an accelerating cosmological model within extended STG, employing a hybrid scale factor constrained by observational data, which reveals a transition from early-time deceleration to late-time acceleration with quintessence-like behavior approaching  $\Lambda$ CDM, while violating the strong energy condition. Narawade et al. [22] proposed an accelerating cosmological model within extended STG, employing a hybrid scale factor constrained by observational data, which reveals a transition from early-time deceleration to late-time acceleration with quintessence-like behavior approaching  $\Lambda$ CDM, while violating the strong energy condition. Lohakare and Mishra [23] proposed a viable alternative to  $\Lambda$ CDM by analyzing  $f(Q, B)$  gravity through a dynamical system and Bayesian inference, revealing a stable de Sitter phase and a smooth transition from deceleration to late-time acceleration consistent with observational data.

The remarkable advancements in cosmology are evidenced by the current rapid expansion of the cosmos. The change in the universe's timeline, known as accelerated expansion, is driven by a paradigm termed as an exotic force, which accommodates a repulsive nature with significant negative pressure. This phenomenon is commonly referred to as DE. It is assumed that this exotic energy will determine the ultimate fate of the cosmos, yet its perplexing characteristics remain unknown. The cosmic accelerating issue is primarily addressed through two main approaches. Modified theories of gravity represent one approach, serving as alternative frameworks for incorporating DE.

Dynamical DE, a captivating idea in cosmology, has spurred exploration of models to understand cosmic expansion. The alteration of matter results not only in scalar field models like **quintessence**, **k-essence** and **phantom fields** [24], but also generates the dynamic DE models such as holographic, agegraphic and pilgrim DE (PDE) models [25]. The DE models at the theoretical level remain consistent with observational data and can be described

using various energy density formulations. As a consequence of energy dissipation, these models avoid the coincidence issue that arises due to the dominance of DE. To prevent the creation of black holes, Wei [26] introduced the PDE model, employing an energy density given by

$$\rho_{DE} = 3\alpha^2 M_p^{4-u} H^u, \quad (1)$$

where  $\alpha$  is non-zero constant,  $H$  represents Hubble parameter,  $M_p$  denotes the Planck mass, and  $u$  is the pilgrim parameter.

The choice of PDE is rooted in its distinct theoretical foundation and relevance to phantom cosmology. Unlike conventional holographic DE models, PDE is designed specifically to account for a universe dominated by phantom energy  $\omega < -1$ , a regime that observational data from Planck and supernova surveys have increasingly supported as a viable scenario for late-time cosmic acceleration. The central idea behind PDE, is that strong phantom energy not only drives accelerated expansion but also has sufficient repulsive force to prevent the formation of black holes. This leads to a scenario where DE acts as a powerful agent against gravitational collapse, setting PDE apart from other DE models. Furthermore, PDE naturally leads to a freezing region in the  $\omega_{DE} - \omega'_{DE}$  plane, which aligns with observational features of DE evolution. Its inclusion in our model allows us to examine whether a geometric theory of gravity specifically  $f(\mathbb{Q}, \mathbb{T})$  gravity that incorporates both non-metricity and matter coupling via  $\mathbb{T}$  can reproduce similar dynamics without exotic fields. By reconstructing the PDE scenario under this modified gravity setup, we provide a deeper insight into how extended gravitational interactions and DE interplay to govern the universe's evolution. This integration of PDE with  $f(\mathbb{Q}, \mathbb{T})$  gravity not only enhances the richness of the theoretical model but also contributes to a more unified framework that can potentially explain both geometric and matter induced acceleration mechanisms. Therefore, the adoption of PDE is both a natural and compelling choice to explore within the scope of extended cosmological models. Sharif and Zubair [27] examined the cosmic expansion of the PDE model using infrared (IR) cutoffs such as the event horizon, particle horizon and the universe's conformal age. Jawad [28] examined the cosmological dynamics of the PDE model within the framework of quantum cosmology, employing the Hubble horizon as an infrared cutoff for the interacting framework.

Modified theories of gravity often utilize the reconstruction phenomenon as a key approach for developing a DE model that can precisely predict

the trajectory of cosmic evolution. In this context, comparisons are made between the respective energy densities of DE and altered gravity theories. As a result, a desired general function of the underlying gravity theory is derived using the correspondence method of energy densities. Chattopadhyay et al. [29] delved into the enigmatic nature of the PDE model in  $f(T, T_{\mathbb{G}})$  ( $\mathbb{G}$  is the *Gauss-Bonnet invariant*) gravity, concluding that an assertive phantom-like behavior for  $u = -2$  (PDE parameter) is crucial to avoid black hole formation. Sharif and Rani [30] constructed a PDE model based on  $f(T)$  gravity, aiming to describe the interactions of black holes with phantom energy throughout the universe. The behavior of the PDE model in  $f(\mathbb{G})$  gravity was examined [31], revealing that the dynamical framework uncovers multiple DE scenarios. Sharif and Shah [32] investigated the dynamics of non-interacting and interacting PDE within a non-flat Friedmann-Robertson-Walker (FRW) model using Brans-Dicke theory. Myrzakulov et al. [33] examined the dynamic behavior of the EoS parameter,  $\omega_D - \omega'_D$  and the statefinder planes using the PDE model in  $f(\mathbb{Q})$  gravity.

This study utilizes a correspondence method to reconstruct the PDE  $f(\mathbb{Q}, \mathbb{T})$  model, with a particular emphasis on a non-interacting scenario. We investigate cosmic evolution by examining the EoS parameter and phase planes. The paper is structured as follows: Section 2 introduces the  $f(\mathbb{Q}, \mathbb{T})$  gravity framework and its associated field equations. Section 3 details the reconstruction approach employed to develop the PDE  $f(\mathbb{Q}, \mathbb{T})$  model. In section 4, we delve into cosmic dynamics by analyzing the EoS and phase planes and we assess the stability of the model through the squared speed of sound ( $\nu_s^2$ ). The paper concludes with a discussion of our research findings.

## 2 Geometrical Basis of $f(\mathbb{Q}, \mathbb{T})$ Gravity

## 3 Reconstruction of PDE $f(\mathbb{Q}, \mathbb{T})$ Model

We consider the uniformly homogeneous and isotropic FRW universe model, described by

$$ds^2 = -dt^2 + \mathbf{a}^2(t)[dx^2 + dy^2 + dz^2], \quad (2)$$

where  $\mathbf{a}$  represents the *scale factor* of the universe. The isotropic matter setup, specified through the four-velocity  $u_\mu$ , along with the normal matter

density ( $\rho_M$ ) and pressure ( $P_M$ ) is expressed as follows

$$\tilde{\mathbb{T}}_{\mu\nu} = P_M g_{\mu\nu} + (\rho_M + P_M) u_\mu u_\nu. \quad (3)$$

The modified Friedmann equations within the framework of  $f(\mathbb{Q}, \mathbb{T})$  theory can be formulated as

$$\rho_M + \rho_{DE} = \rho_{eff} = 3H^2, \quad (4)$$

$$P_M + P_{DE} = P_{eff} = 2\dot{H} + 3H^2, \quad (5)$$

where  $H = \frac{\dot{\mathbf{a}}}{\mathbf{a}}$ , with the dot notation indicating differentiation with respect to the universal time  $t$ . The expression for  $\mathbb{Q}$  in relation to the Hubble parameter is given by

$$\mathbb{Q} = -\frac{1}{4} \left[ -\mathbb{Q}_{\rho\xi\eta} \mathbb{Q}^{\rho\xi\eta} + 2\mathbb{Q}_{\rho\xi\eta} \mathbb{Q}^{\xi\rho\eta} - 2\tilde{\mathbb{Q}}^\rho \mathbb{Q}_\rho + \mathbb{Q}^\rho \mathbb{Q}_\rho \right], \quad (6)$$

which can be simplified to

$$\mathbb{Q} = 6H^2. \quad (7)$$

Furthermore,  $\rho_{DE}$  and  $P_{DE}$  denote the DE density and pressure and are given by

$$\rho_{DE} = \frac{1}{2} f(\mathbb{Q}, \mathbb{T}) - f_{\mathbb{T}}(\rho_M + P_M) - \mathbb{Q} f_{\mathbb{Q}}, \quad (8)$$

$$P_{DE} = -\frac{1}{2} f(\mathbb{Q}, \mathbb{T}) + 2f_{\mathbb{Q}} \dot{H} + \mathbb{Q} f_{\mathbb{Q}} + 2f_{\mathbb{Q}\mathbb{Q}} H. \quad (9)$$

For an ideal fluid, the non-conservation equation (??) assumes the following expression

$$3H(\rho_M + P_M) + \dot{\rho}_M = \frac{1}{(f_{\mathbb{T}} - 1)} \left[ 2\nabla_\beta (P_M \mu^\beta f_{\mathbb{T}}) + f_{\mathbb{T}} \nabla_\beta \mu^\beta \mathbb{T} + 2\mu^\beta \mathbb{T}_{\alpha\beta} \nabla^\alpha f_{\mathbb{T}} \mu^\beta \right]. \quad (10)$$

With reference to the (4), it follows that

$$\Omega_{DE} + \Omega_M = 1, \quad (11)$$

In this framework,  $\Omega_M = \frac{\rho_M}{3H^2}$  and  $\Omega_{DE} = \frac{\rho_{DE}}{3H^2}$  depict the fractional energy densities of normal matter and DE, respectively. Cosmological models that incorporate dynamic DE, whose energy density is directly related to the

Hubble parameter, are essential for understanding the observed rapid expansion of the universe. In this study, we focus on the non-interacting case to establish the core properties and stability of the PDE model in  $f(\mathbb{Q}, \mathbb{T})$  gravity. Moving forward, we will apply a correspondence method within an ideal fluid framework to develop the PDE  $f(\mathbb{Q}, \mathbb{T})$  gravity model for a dust scenario where  $P_M = 0$

### 3.1 Non-interacting PDE $f(\mathbb{Q}, \mathbb{T})$ Model

In this section, we delve into the standard formulation of the  $f(\mathbb{Q}, \mathbb{T})$  function as outlined in [37]

$$f(\mathbb{Q}, \mathbb{T}) = f_1(\mathbb{Q}) + f_2(\mathbb{T}). \quad (12)$$

Under these conditions, the interaction between the matter components and curvature is minimal. This specific version of the generic function denotes an entirely gravitational interaction, making it easy to handle. This provides a detailed explanation for the universe ongoing expansion. Furthermore, the reconstruction process confirms that the resulting models are consistent with physical principles [37]. By applying Eq.(12), the field equations (4) and (5) lead to the following

$$\rho_M + \rho_{DE} = \rho_{eff} = 3H^2, \quad P_{DE} = P_{eff} = 2\dot{H} + 3H^2, \quad (13)$$

where

$$\rho_{DE} = \frac{1}{2}f_1(\mathbb{Q}) - \mathbb{Q}f_{1\mathbb{Q}} + \frac{1}{2}f_2(\mathbb{T}) + f_{2\mathbb{T}}\rho_M, \quad (14)$$

$$P_{DE} = -\frac{1}{2}f_1(\mathbb{Q}) - \frac{1}{2}f_2(\mathbb{T}) + 2f_{1\mathbb{Q}}\dot{H} + 2f_{1\mathbb{Q}\mathbb{Q}}H + \mathbb{Q}f_{1\mathbb{Q}}. \quad (15)$$

The related conservation equation (10) simplifies to

$$\dot{\rho}_M + 3H\rho_M = \frac{1}{f_{2\mathbb{T}} - 1} [2\mathbb{T}f_{2\mathbb{T}\mathbb{T}} + f_{2\mathbb{T}}\dot{\mathbb{T}}]. \quad (16)$$

This equation reduces to the conventional continuity equation when the right-hand side is annulled, indicating that

$$3H\rho_M + \dot{\rho}_M = 0 \quad \implies \quad \mathbf{a}(t)^{-3}\rho_0 = \rho_M, \quad (17)$$

with the constraint

$$f_{2\mathbb{T}} + 2\mathbb{T}f_{2\mathbb{T}\mathbb{T}} = 0, \quad (18)$$

whose approach yields

$$f_2(\mathbb{T}) = B_1 \mathbb{T}^{\frac{1}{2}} + B_2, \quad (19)$$

where  $\rho_0$ ,  $B_1$  and  $B_2$  represent the integration constants. For  $M_p^{4-u} = 1$  in Eq.(1), we obtain

$$\rho_{DE} = 3\alpha^2 H^u. \quad (20)$$

The addition of the PDE model within the modified  $f(\mathbb{Q}, \mathbb{T})$  gravity framework complements the geometrical modification of the Einstein-Hilbert action by providing a practical mechanism for detailed cosmic diagnostics and aligning with observational data on DE. While the modified Einstein-Hilbert action addresses cosmic acceleration theoretically, the PDE model enables a focused examination of DE dynamics, such as the EoS and stability. By allowing specific empirically testable scenarios, the PDE model enhances the robustness and observational consistency of  $f(\mathbb{Q}, \mathbb{T})$  gravity, particularly in describing late-time acceleration and phantom behavior, ultimately creating a more comprehensive framework for understanding DE. We employ Eqs.(14) and (20) along with the constraint on  $f_2(\mathbb{T})$  provided in (19) to develop a reconstruction framework using the correspondence method

$$\frac{f_1(\mathbb{Q})}{2} - \mathbb{Q}f_{1\mathbb{Q}} + B_1 \mathbb{T}^{\frac{1}{2}} + \frac{1}{2}B_2 = 3\alpha^2 H^u, \quad (21)$$

or

$$f_1(\mathbb{Q}) - 2\mathbb{Q}f_{1\mathbb{Q}} + 2B_1 \mathbb{T}^{\frac{1}{2}} + B_2 = 6\alpha^2 H^u, \quad (22)$$

where  $g_1 = 6\alpha^2$  is an arbitrary constant.

We apply the *power-law* solution for the *scale factor*, presented as

$$\mathbf{a}(t) = \mathbf{a}_0 t^m, \quad m > 0. \quad (23)$$

Here,  $\mathbf{a}_0$  denotes the present scale factor. In this study, we have chosen the power-law form for the scale factor, for several well-justified reasons. Mathematically, this form greatly simplifies the structure of the field equations within the modified gravity framework, particularly in the context of  $f(\mathbb{Q}, \mathbb{T})$  gravity, enabling direct analytical solutions that are otherwise challenging to obtain. This analytical tractability facilitates a clearer and more systematic investigation of cosmic dynamics. Additionally, power-law cosmology is widely used in gravitational models, as it effectively encapsulates various key evolutionary phases of the universe including radiation-dominated, matter-dominated, and accelerated expansion epochs. Its flexibility allows

a smooth interpolation between these phases, providing a robust and interpretable structure for modeling the behavior of DE. Moreover, the power-law form proves advantageous for qualitative studies, such as examining the evolution of the EoS, conducting phase space analysis, and testing stability conditions. While it represents a specific class of solutions, it serves as a reasonable approximation for late-time cosmology and yields insights that are qualitatively consistent with broader dynamical models. It also supports effective comparison with observational data, thus enhancing the model's testability and reliability.

Using this relationship,  $H$ , its derivative and the  $\mathbb{Q}$  can be expressed as functions of cosmic time  $t$  as

$$\mathbb{Q} = 6\frac{m^2}{t^2}, \quad H = \frac{m}{t}, \quad \dot{H} = -\frac{m}{t^2}.$$

Substituting Eq.(23) into (17), it can be concluded that

$$\rho_M = \rho_0(\mathbf{a}_0 t^m)^{-3}. \quad (24)$$

By applying Eq.(23) to (22), the function  $f_1(\mathbb{Q})$  can be determined as

$$f_1(\mathbb{Q}) = \sqrt{\mathbb{Q}} \left[ 4 \left\{ \frac{a\sqrt{\mathbb{T}} 2^{\frac{3m}{8}+2} 3^{\frac{3m}{8}} \left( \frac{\mathbb{Q}}{m^2} \right)^{-\frac{3m}{8}}}{(3m+4)\sqrt{\mathbb{Q}}} + \frac{g_1 6^{-u} m^{-u} \mathbb{Q}^{u+\frac{1}{2}}}{2u+1} \right\} + \frac{2b}{\sqrt{\mathbb{Q}}} \right] + g_2 \sqrt{\mathbb{Q}}, \quad (25)$$

where  $g_2$  is the integration constant,  $a$  and  $b$  are arbitrary constant. As a result, the reconstructed  $f(\mathbb{Q}, \mathbb{T})$  framework is derived by inserting Eqs.(19) and (25) into (12), yielding the following expression

$$f(\mathbb{Q}, \mathbb{T}) = \sqrt{\mathbb{Q}} \left[ 4 \left\{ \frac{a\sqrt{\mathbb{T}} 2^{\frac{3m}{8}+2} 3^{\frac{3m}{8}} \left( \frac{\mathbb{Q}}{m^2} \right)^{-\frac{3m}{8}}}{(3m+4)\sqrt{\mathbb{Q}}} + \frac{g_1 6^{-u} m^{-u} \mathbb{Q}^{u+\frac{1}{2}}}{2u+1} \right\} + \frac{2b}{\sqrt{\mathbb{Q}}} \right] + B_1 \sqrt{\mathbb{T}} + B_2 + g_2 \sqrt{\mathbb{Q}}. \quad (26)$$

For the sake of simplicity, we have taken  $\mathbb{T} = \rho_0$ .

Next, we express this function with respect to the redshift parameter  $z$ . The deceleration parameter  $q$  is subsequently defined by

$$q = -\frac{\mathbf{a}\ddot{\mathbf{a}}}{\dot{\mathbf{a}}^2}. \quad (27)$$

The progression of the cosmic *scale factor*, with respect to  $q$ , is outlined as

$$\mathbf{a}(t) = t^{(1+q)^{-1}}, \quad (28)$$

where  $q = -0.831_{-0.091}^{+0.091}$  [38]. In this context, we assume  $\mathbf{a}_0$  to be unity [39]. The frequent use of the *power-law* form in cosmological models is justified for several reasons. Its mathematical simplicity facilitates straightforward analytical calculations, making it easier to derive and analyze equations describing the universe's evolution. The *power-law* model indicates that the universe is expanding when the  $q$  is greater than -1. Moreover, *power-law* solutions naturally arise from the equations in some modified gravity theories and specific cosmological models. The essential characteristics of the expansion stage and the current cosmological development are outlined below

$$H = t^{-1}(1+q)^{-1}, \quad H_0 = (q+1)^{-1}t_0^{-1}. \quad (29)$$

Within *power-law* cosmology, the expansion dynamics of the cosmos are governed by two key factors: the Hubble constant  $H_0$  and  $q$ . By exploring the relationship between  $\mathbf{a}$  and  $z$ , we are able to

$$H = H_0 \Upsilon^{1+q}, \quad (30)$$

here  $\Upsilon = z + 1$ . Substituting Eq.(30) into (7),  $\mathbb{Q}$  can be expressed as follows

$$\mathbb{Q} = 6H_0^2 \Upsilon^{2+2q}. \quad (31)$$

Figure 1 presents the deceleration parameter versus redshift for three different values of  $m$ , showing a decreasing trend with redshift. The parameter transitions into negative values, which correspond to the accelerating phase of the universe. This behavior aligns well with current observational data, thereby supporting the physical validity of our model. Figure 2 illustrates the evolution of the Hubble parameter with redshift for different values of  $m$ . As expected, the Hubble parameter shows positive behavior and an increasing trend with redshift, which is consistent with observational data and confirms that the model accurately captures the universe expansion dynamics. Substituting this value into Eq.(26), we obtain the reconstructed solution for the PDE  $f(\mathbb{Q}, \mathbb{T})$  as it relates to the redshift parameter, leading to

$$f(\mathbb{Q}, \mathbb{T}) = \frac{16a\sqrt{\rho_0}\left(\frac{\beta^2\Upsilon^{2q+2}}{m^2}\right)^{-\frac{3m}{8}}}{3m+4} + 2b + \frac{24g_1m^{-u}\left(\beta^2\Upsilon^{2q+2}\right)^{u+1}}{2u+1}$$

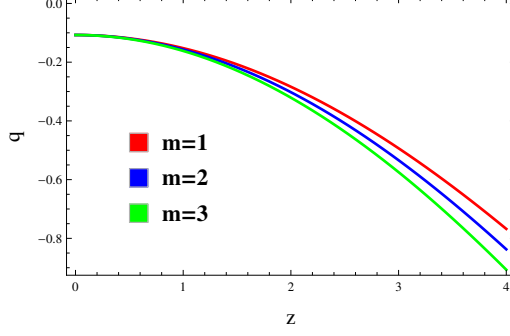


Figure 1: Graph of  $q$  versus  $t$ .

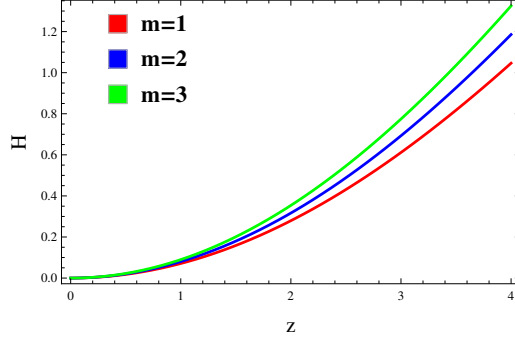


Figure 2: Graph of  $H$  versus  $t$ .

$$+ B_1\sqrt{\rho_0} + B_2 + \sqrt{6}g_2\sqrt{\beta^2\Upsilon^{2q+2}}. \quad (32)$$

In the graphical examination, the parameters are fixed at  $a = 5$ ,  $b = 1$  and  $u = \pm 2$ . As illustrated in Figure 3, the reconstructed PDE  $f(Q, T)$  framework exhibits a consistent decline for  $u = 2$  and an upward trend for  $u = -2$ . Figures 4 and 5 illustrate the variation of  $\rho_{DE}$  and  $P_{DE}$  with the redshift parameter. The  $\rho_{DE}$  exhibits an increase, while  $P_{DE}$  stays negative across all values of  $u$  and  $m$ , aligning with the expected dynamics of DE. These attributes are further scrutinized within the reconstructed PDE  $f(Q, T)$  framework. By substituting (32) into (14) and (15), the following results are obtained

$$\rho_{DE} = 2a\sqrt{\rho_0}\left(\frac{H_0^2\Upsilon^{2q+2}}{m^2}\right)^{-\frac{3m}{8}} + b + B_1\rho_0^{3/2} + B_1\sqrt{\rho_0} + B_2\rho_0 + B_2 - 12g_1m^{-u}$$

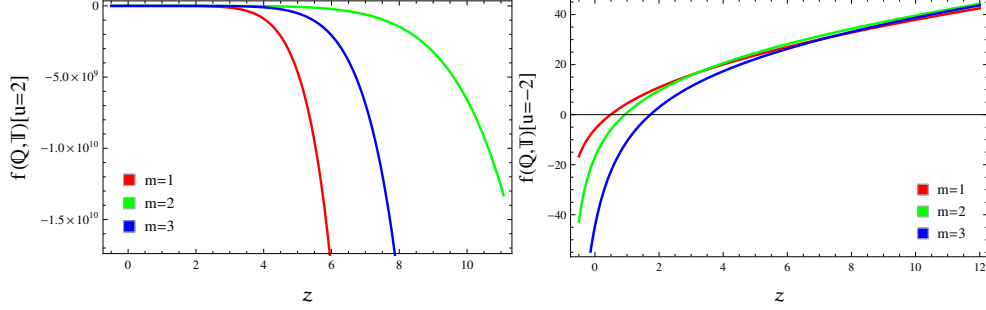


Figure 3: Graph of the DE  $f(\mathbb{Q}, \mathbb{T})$  model corresponding to  $u = \pm 2$  as a function of  $z$ .

$$\begin{aligned}
& \times \left( H_0^2 \Upsilon^{2q+2} \right)^{u+1}, \\
P_{DE} = & \left[ m^{-u} \Upsilon^{-3(q+1)} \left( \frac{H_0^2 \Upsilon^{2q+2}}{m^2} \right)^{-\frac{3m}{8}} (2u+1) m^u \left( 3a\sqrt{\rho_0} \left\{ -144H_0^3 m \Upsilon^{3q+3} \right. \right. \right. \\
& - 48H_0^2 (4H_0 - m) (\Upsilon^{3q+3} + m(3m+8)) \left. \left. \right) - 36H_0^3 (3m+4) \Upsilon^{3q+3} \left( \frac{H_0^2 \Upsilon^{2q+2}}{m^2} \right)^{\frac{3m}{8}} \right. \\
& \times \left\{ 2b + B_1 \sqrt{\rho_0} + B_2 \right\} - \sqrt{6} g_2 (3m+4) \sqrt{H_0^2 \Upsilon^{2q+2}} (12H_0^2 \Upsilon^{3q+3} + 1) \\
& \times \left( \frac{H_0^2 \Upsilon^{2q+2}}{m^2} \right)^{\frac{3m}{8}} \left. \right\} - 24g_1 H_0 (3m+4) \Upsilon^{q+1} \left( \frac{H_0^2 \Upsilon^{2q+2}}{m^2} \right)^{\frac{3m}{8}} (H_0^2 \Upsilon^{2q+2})^u \\
& \times \left\{ -72H_0^4 (u+1) \Upsilon^{4q+4} + 24H_0^3 (u+1) \Upsilon^{4q+4} - 4H_0 u (u+1) \Upsilon^{q+1} \right. \\
& \left. \left. + 36H_0^4 \Upsilon^{4q+4} \right\} \right] \left[ 72H_0^3 (3m+4) (2u+1) \right]^{-1}.
\end{aligned}$$

## 4 Cosmological Examination

This section of the study delves into the cosmological development of the universe across various epochs. We employ the reconstructed PDE  $f(\mathbb{Q}, \mathbb{T})$  framework within a non-interacting context, as elaborated in Eq.(32). Additionally, the evolution of critical cosmological parameters, including the EoS,

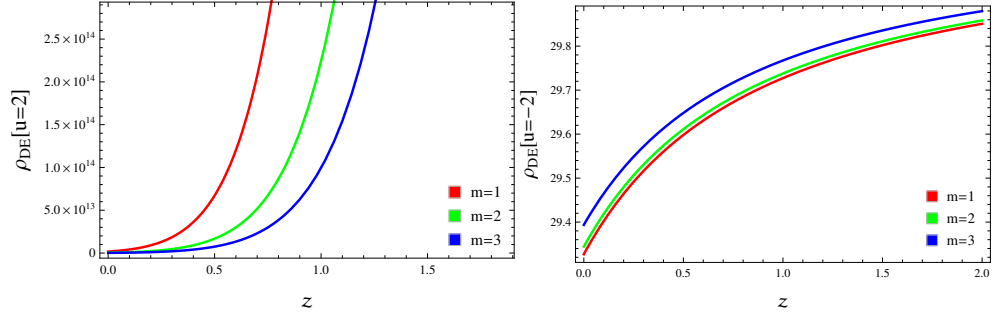


Figure 4: Graphs of  $\rho_{DE}$  ( $u = \pm 2$ ) versus  $z$ .

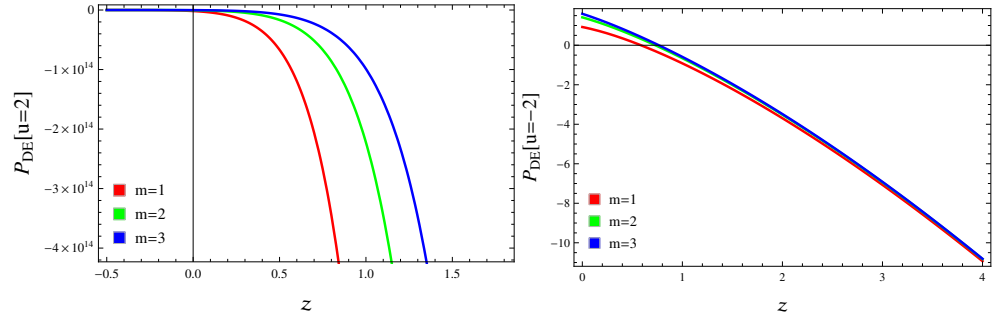


Figure 5: Graphs of  $P_{DE}$  ( $u = \pm 2$ ) against  $z$ .

the  $\omega_{DE} - \omega'_{DE}$  plane and the statefinder planes, is illustrated. The stability of the framework is rigorously assessed as well.

## 4.1 The EoS Parameter

The EoS parameter, denoted by  $\omega = \frac{P_{DE}}{\rho_{DE}}$ , is essential for understanding both the phase of cosmic inflation and the universe's ongoing expansion. We examine the conditions required for a universe to accelerate, which occurs when  $\omega$  is less than  $-\frac{1}{3}$ . Specifically,  $\omega = -1$  corresponds to the cosmological constant, while  $\omega = \frac{1}{3}$  and  $\omega = 0$  represent a universe dominated by radiation and matter, respectively. Additionally, the phantom regime emerges when  $\omega$  falls below -1. The EoS parameter is formulated as follows

$$\omega_{DE} = \frac{P_{eff}}{\rho_{eff}} = \frac{P_{DE}}{\rho_{DE} + \rho_M}. \quad (33)$$

Equations (14), (15), and (24) are applied to the above expression to calculate the relevant parameter as follows

$$\begin{aligned} \omega_{DE} = & 2^{-\frac{3m}{8}-u-\frac{7}{2}} 3^{-\frac{3m}{8}-u-\frac{5}{2}} m^{-u} \left( \frac{H_0^2 \Upsilon^{2q+2}}{m^2} \right)^{-\frac{3m}{8}} \left[ 6^{u+\frac{1}{2}} (2u+1) m^u \sqrt{H_0^2 \Upsilon^{2q+2}} \right. \\ & \times \left\{ a \sqrt{\rho_0} 6^{\frac{3m}{8}} \left( -432 H_0^4 m \Upsilon^{4q+4} - 48 H_0^2 \Upsilon^{2q+2} (12 H_0^2 \Upsilon^{2q+2} - 3 H_0 m \Upsilon^{2q+2}) \right. \right. \\ & + 3 H_0 m (3m+8) \Upsilon^{q+1} \left. \left. + H_0^4 6^{\frac{3m}{8}+2} (3m+4) \Upsilon^{4q+4} \left( \frac{H_0^2 \Upsilon^{2q+2}}{m^2} \right)^{\frac{3m}{8}} \left\{ -2b \right. \right. \right. \\ & - B_1 \sqrt{\rho_0} - B_2 \left. \left. \right\} - g_2 6^{\frac{3m}{8}+\frac{1}{2}} (3m+4) \sqrt{H_0^2 \Upsilon^{2q+2}} \left\{ -36 H_0^4 \Upsilon^{4q+4} + 6 H_0^2 \Upsilon^{2q+2} \right. \right. \\ & \times (6 H_0^2 \Upsilon^{2q+2} + 2 H_0 \Upsilon^{2q+2}) + H_0 \Upsilon^{q+1} \left. \left. \right\} \left( \frac{H_0^2 \Upsilon^{2q+2}}{m^2} \right)^{\frac{3m}{8}} \right\} \times 2^{\frac{3m}{8}+u+\frac{7}{2}} 3^{\frac{3m}{8}+u+\frac{3}{2}} \\ & - g_1 (3m+4) \left( \frac{H_0^2 \Upsilon^{2q+2}}{m^2} \right)^{\frac{3m}{8}} (H_0^2 \Upsilon^{2q+2})^{u+\frac{3}{2}} \left( -72 H_0^4 (u+1) \Upsilon^{4q+4} \right. \\ & + 36 H_0^4 \Upsilon^{4q+4} + 24 H_0^3 (u+1) \Upsilon^{4q+4} - 4 H_0 u (u+1) \Upsilon^{q+1} \left. \right) \left[ (3m+4) \right. \\ & \times (2u+1) (H_0^2 \Upsilon^{2q+2})^{5/2} \left\{ 2a \sqrt{\rho_0} \left( \frac{H_0^2 \Upsilon^{2q+2}}{m^2} \right)^{-\frac{3m}{8}} + b + B_1 \sqrt{\rho_0} \right. \end{aligned}$$

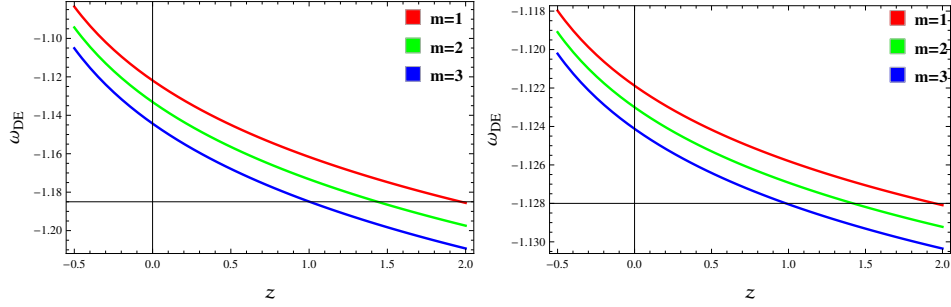


Figure 6: Graph of the EoS parameter for  $u = \pm 2$  versus  $z$ .

$$+ B_2 - 12g_1 m^{-u} \left( H_0^2 \Upsilon^{2q+2} \right)^{u+1} \Big\}.$$

Figure 6 illustrates the dynamics of the EoS parameter as a function of  $z$ , demonstrating that both  $u = 2$  and  $u = -2$  align with a phantom epoch throughout the present and ensuing stages of cosmic evolution.

## 4.2 $\omega_{DE} - \omega'_{DE}$ Plane

Here, we examine the  $\omega_{DE} - \omega'_{DE}$  plane ( $\omega'_{DE}$  represents the evolution of  $\omega_{DE}$ , while the prime denotes differentiation in terms of  $\mathbb{Q}$ ). Caldwell and Linder [40] introduced a phase plane to analyze the cosmic expansion within the quintessence DE model. Their findings showed that the plane can be separated into two unique regions, thawing ( $\omega_{DE} < 0, \omega'_{DE} > 0$ ) and freezing ( $\omega_{DE} < 0, \omega'_{DE} < 0$ ). In depicting the current model of cosmic expansion, the freezing region indicates a more rapid rate of acceleration as compared to the thawing region. Figure 7 presents the cosmic trajectories in the  $\omega_{DE} - \omega'_{DE}$  plane, illustrating the universe freezing phase under specific values of the parameters  $m$  and  $u$ . In this phase, the conditions  $\omega_{DE} < 0$  and  $\omega'_{DE} < 0$  are satisfied, indicating that the rate of cosmic expansion is accelerating. The expression for  $\omega'_{DE}$  can be found in Appendix A.

## 4.3 $r - s$ Plane

The deceleration and Hubble parameters provide a clear description of the evolving cosmos. Nevertheless, numerous DE models have identical parametric values at present. A set of unitless cosmological parameters known as

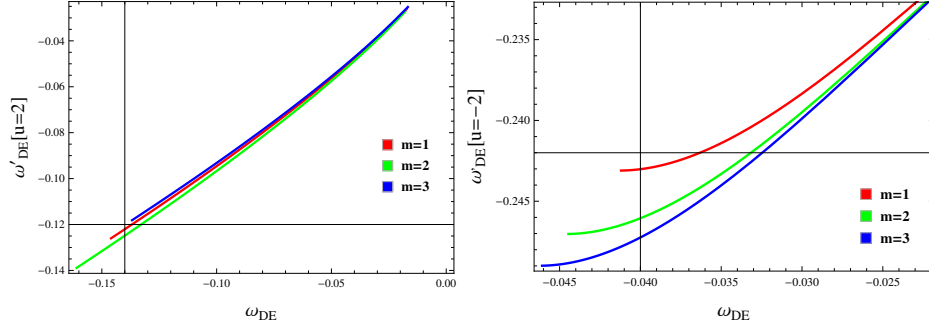


Figure 7:  $\omega_{DE} - \omega'_{DE}$  ( $u = \pm 2$ ) against  $z$ .

statefinders, derived from the deceleration and Hubble parameters, is used to classify DE models, as [41]

$$r = \frac{\ddot{a}}{aH^3}, \quad s = \frac{r-1}{3(q-\frac{1}{2})}. \quad (34)$$

The parameter  $r$  is defined with respect to the deceleration parameter as follows

$$r = 2q^2 + q - \dot{q}. \quad (35)$$

The parameter  $s$  controls the speed of cosmic acceleration, whereas the parameter  $r$  reflects variations from a strict *power-law* expansion. The dynamics of this diagnostic pair is crucial for illustrating different cosmic phases and distinguishing between various DE models. When  $(r, s) = (1, 0)$ , it signifies the cold dark matter (CDM) regime, whereas  $(r, s) = (1, 1)$  corresponds to the  $\Lambda$ CDM model. The region where  $r < 1$  and  $s > 0$  includes both phantom and non-phantom phases, while the Chaplygin gas (CG) model is defined by  $r > 1$  and  $s < 0$ . Figure 8 illustrates the  $r - s$  phase plane, showing  $r > 1$  and  $s < 0$ , which verifies the presence of the CG model. This indicates that our model effectively captures the universe's transition to an accelerating expansion, consistent with observational evidence of cosmic acceleration.

#### 4.4 $\nu_s^2$ Parameter

The stability of the DE framework can be directly evaluated using perturbation theory by analyzing the sign of the  $\nu_s^2$  parameter. In this context, we

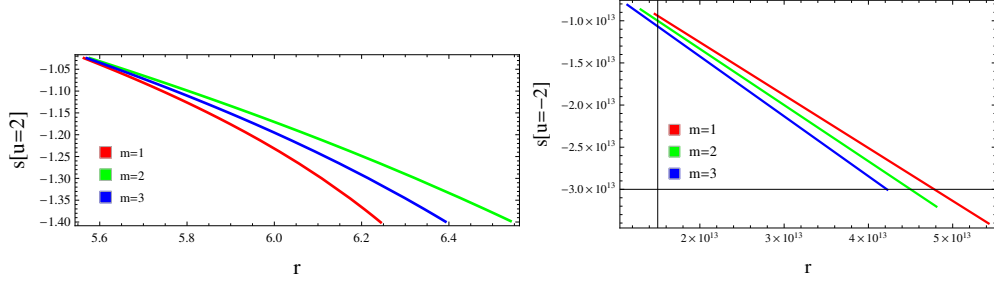


Figure 8: Graph of the  $r - s$  plane for  $u = \pm 2$  as a function of  $z$ .

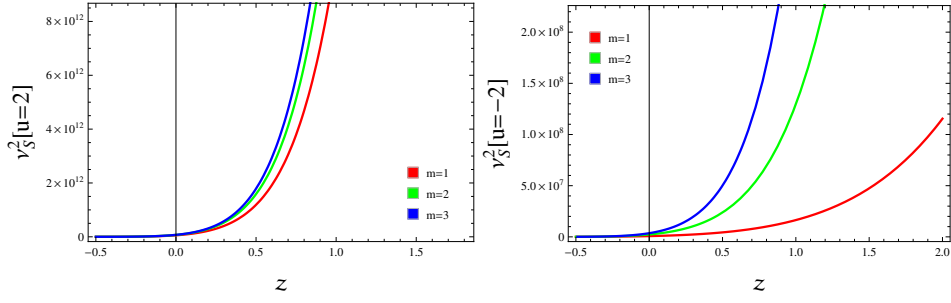


Figure 9: Plot of  $\nu_s^2$  ( $u = \pm 2$ ) versus  $z$ .

examine the  $\nu_s^2$  to evaluate the stability of the PDE  $f(\mathbb{Q}, \mathbb{T})$  approach, as outlined [42]

$$\nu_s^2 = \frac{P'_{eff}}{\rho'_{eff}}. \quad (36)$$

A positive value indicates that the configuration is stable, while a negative value points to instability within the associated framework. By substituting the required expressions into the equation for the reconstructed framework, we obtain the  $\nu_s^2$  parameter, which is elaborated upon in Appendix **B**. As shown in Figure **9**, all tested values of  $m$  and  $u$  demonstrate positive behavior, validating the stability of the reconstructed  $f(\mathbb{Q}, \mathbb{T})$  DE framework during the universe's evolution. This stability across varying parameters highlights the framework's robustness and its capability to represent a consistent cosmic evolution.

## 4.5 Jerk, Snap, Lerk and Maxout parameters

One of the central challenges in modern cosmology is distinguishing between a cosmological constant and alternative DE models as explanations for the universe accelerated expansion. To develop robust, model-independent diagnostic tools, it becomes essential to examine cosmographic parameters that extend beyond the deceleration parameter. These include the jerk, snap, lerk, and maxout parameters, which provide a higher-order description of cosmic kinematics. These cosmographic quantities are derived from successive time derivatives of the scale factor and serve to refine our understanding of deviations from standard cosmological scenarios. Specifically, they are defined as:

$$\begin{aligned} J &= \frac{1}{aH^3} \frac{d^3 a}{dt^3}, & S &= \frac{1}{aH^4} \frac{d^4 a}{dt^4}, \\ L &= \frac{1}{aH^5} \frac{d^5 a}{dt^5}, & M &= \frac{1}{aH^6} \frac{d^6 a}{dt^6}, \end{aligned} \quad (37)$$

where  $J, S, L, M$  correspond to the jerk, snap, lerk and maxout parameters, respectively. These higher order descriptors offer a detailed perspective on the universe expansion dynamics, extending the traditional cosmographic series composed of the Hubble and deceleration parameters. While they emerge from the scale factor's derivatives, they also relate closely to higher order derivatives of position or displacement in kinematic terms, thus playing a vital role in the dynamical analysis of cosmic evolution. Notably, these parameters are not mutually independent but are interconnected through well defined mathematical relationships. Figure 10 illustrates the evolution of these cosmographic indicators, revealing a positive trend consistent with ongoing cosmic acceleration. Moreover, their behavior mirrors key features expected from the  $\Lambda$ CDM model, lending further credibility to its framework within observational limits.

## 5 Summary

This study explores the features of the PDE model for a *power law scale factor* of the flat FRW universe. We have applied a reconstruction approach through the correspondence principle within  $f(\mathbb{Q}, \mathbb{T})$  theory. The reconstructed PDE  $f(\mathbb{Q}, \mathbb{T})$  model's cosmic evolutionary paradigm has been assessed using cosmological parameters. To assess the effects of  $\mathbb{Q}$  and  $\mathbb{T}$  within the PDE

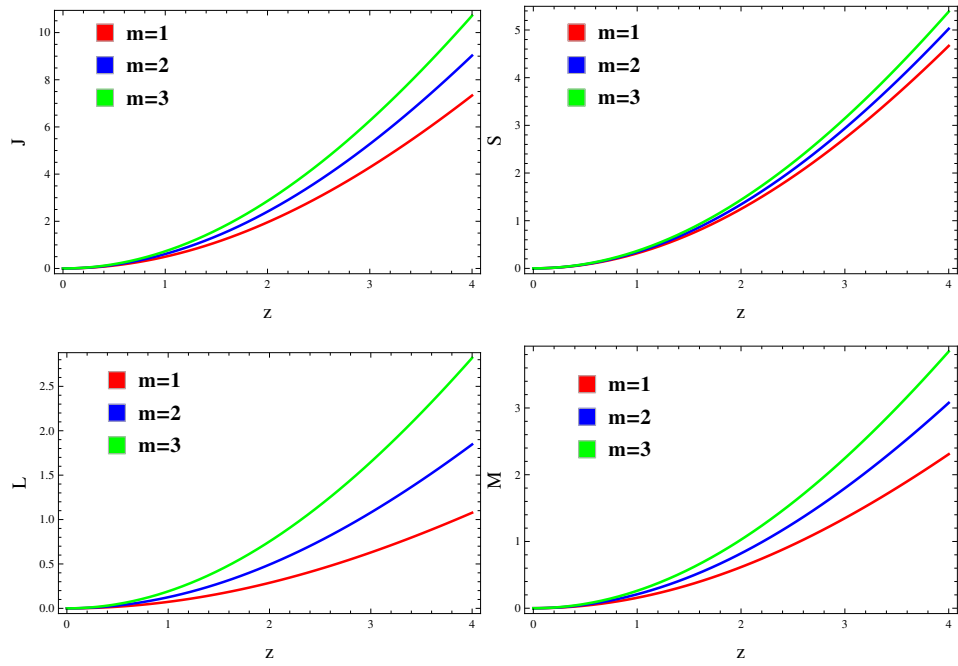


Figure 10: Graphs of Jerk, Snap, Lerk and Maxout against  $z$ .

framework, we have a selected model of this theory. We have reconstructed  $f(\mathbb{Q}, \mathbb{T})$  models based on two PDE parameter values  $u = \pm 2$ . We have then examined the equation of state parameter,  $\omega_{DE} - \omega'_{DE}$ , along with the statefinder planes. Lastly, we assessed the stability of the derived paradigm by analyzing the  $\nu_s^2$  parameter. Here is a summary of the main results.

- The reconstructed PDE  $f(\mathbb{Q}, \mathbb{T})$  model exhibits a decreasing and increasing trend in  $z$  when  $u = 2$  and  $u = -2$ , respectively that satisfy the monotonic property of pilgrim parameters (Figure 3).
- The  $\rho_{DE}$  displays positive behavior, marked by an increase, whereas the  $P_{DE}$  shows negative behavior. These patterns align closely to the properties of DE (Figures 4 and 5).
- The EoS parameter reveals a phantom phase in the non interacting scenario (Figure 6).
- The developmental path in the  $\omega_{DE} - \omega'_{DE}$  plane indicates a freezing region across every value of  $m$  and  $u$  (Figure 7). This finding supports the conclusion that the non interacting DE  $f(\mathbb{Q}, \mathbb{T})$  gravity predicts a universe with rapid acceleration.
- The  $r - s$  plane illustrates the consistency of the CG framework, where  $r$  and  $s$  fulfill the specified requirements for the model (Figure 8).
- Our analysis shows that the  $\nu_s^2$  parameter is positive, indicating that the PDE  $f(\mathbb{Q}, \mathbb{T})$  gravity is stable across all variations of  $m$  and  $u$  (Figure 9).

The realization of inflation within the PDE model in  $f(\mathbb{Q}, \mathbb{T})$  gravity is theoretically feasible, as this modified framework supports alternative cosmological behavior beyond GR. Unlike standard inflation, the geometric modifications in  $f(\mathbb{Q}, \mathbb{T})$  gravity can naturally induce accelerated expansion. Phase plane analysis through  $\omega_{DE} - \omega'_{DE}$  and statefinder planes, reveals freezing behavior and the CG model, respectively, where rapid acceleration stabilizes over time, a feature consistent with both early cosmic inflation and late time acceleration phases. Notably, the model's phantom regime,  $\omega_{DE} < -1$ , aligns with conditions conducive to inflation and the stability of the model is confirmed by positive  $\nu_s^2$ , indicating its ability to maintain stable configurations

across cosmic phases. This is essential, enabling controlled expansion without disruptive instabilities, a key criterion for successful inflationary behavior.

In conclusion, the results of our study align with the latest observational data, as detailed below [43]

$$\begin{aligned}\omega_{DE} &= -1.023^{+0.091}_{-0.096} \quad (\text{Planck TT+LowP+ext}), \\ \omega_{DE} &= -1.006^{+0.085}_{-0.091} \quad (\text{Planck TT+LowP+lensing+ext}), \\ \omega_{DE} &= -1.019^{+0.075}_{-0.080} \quad (\text{Planck TT, TE, EE+LowP+ext}).\end{aligned}$$

We have derived our results using a range of observational methods with a 95% degree of certainty, ensuring that the statefinder parameters employed for cosmic diagnostics in our framework align with configurational constraints and cosmic boundaries established in previous studies [44]. While prior works in  $f(T)$ ,  $f(Q)$  and  $f(G, T)$  theories of gravity have explored similar themes, our study builds upon these efforts to address gaps and offer new insights. Sharif and Rani [30] investigated  $f(T)$  gravity with an interacting PDE model, revealing a phantom era for certain pilgrim parameter ranges, freezing regions in the  $\omega_{DE} - \omega'_{DE}$  plane and a  $\Lambda$ CDM limit in the statefinder plane. Myrzakulov et al. [33] reconstructed  $f(Q)$  gravity using a power law cosmology to examine PDE in an interacting scenario but lacked emphasis on stability analysis. Sharif and Saba [45] analyzed  $f(G, T)$  gravity via a correspondence method, identifying accelerated expansion and phantom like behavior. In contrast, our study employs  $f(Q, T)$  gravity, where non-metricity plays a central role, setting it apart from the  $f(T)$  and  $f(G, T)$  approaches. We have presented a comprehensive, non-interacting PDE framework, supported by detailed phase plane analysis, revealing a freezing region in the  $\omega_{DE} - \omega'_{DE}$  plane and CG behavior in the  $r - s$  plane, consistent with observational data. Additionally, our model emphasizes stability through the  $\nu_s^2$ , providing a robust analysis often overlooked in the earlier studies. The PDE aims to provide insights into the dynamics of the universe and by applying  $f(Q, T)$  gravity, we offer a promising avenue for addressing key cosmological issues and understanding its long term evolution. Our findings align strongly with recent observational evidence, making this work a significant contribution that complements and extends previous studies in modified gravity frameworks.

Our approach explored key cosmological parameters including the EoS  $\omega_{DE}$ , phase space diagnostics, and the stability parameter  $\nu_s^2$ . A crucial aspect of our formulation lies in the geometrical foundation of the theory

specifically, the non-metricity scalar  $\mathbb{Q} = 6H^2$ , which governs the gravitational action. Through the redshift evolution of  $H(z)$ , we indirectly traced the behavior of  $Q(z)$ , which plays a pivotal role in shaping the dynamical features of the universe in this model. The reconstructed  $f(\mathbb{Q}, \mathbb{T})$  function exhibited consistent behavior with cosmological expectations: the derived  $f(\mathbb{Q}, \mathbb{T})$  decreases with redshift, representing a universe transitioning from a decelerated expansion phase in the past to accelerated expansion at present. This dynamic aligns with current observational constraints, including Planck data that favor a DE EoS near  $\omega_{DE} \approx -1$ . Furthermore, the geometrical quantity  $\mathbb{Q}$  facilitated a natural phantom regime without invoking exotic fields, confirming that the late time acceleration and phantom behavior are geometrically driven. Therefore, our results demonstrate that the geometrical evolution of non metricity within the  $f(\mathbb{Q}, \mathbb{T})$  framework not only supports a stable cosmic scenario but also aligns with contemporary observational data, validating the theoretical robustness of the proposed model.

We have compared the predictions of our reconstructed  $f(\mathbb{Q}, \mathbb{T})$  gravity model with recent cosmological observations provided by the DE spectroscopic instrument (DESI). Our model predicts a phantom-like EoS parameter, where  $\omega_{DE} < -1$ , a feature that remains well within the observational bounds reported by DESI. Specifically, DESI 2024 data release constrains the DE EoS to  $\omega_{DE} = -1.01 \pm 0.06$ , which is consistent with the phantom regime predicted in our framework. Moreover, the redshift-dependent behavior of the Hubble parameter derived from our power-law cosmology aligns closely with the DESI measurements across the range  $0.1 < z < 2$ , where DESI has provided high-precision expansion rate data using baryon acoustic oscillations and redshift-space distortions. Our model naturally exhibits a smooth transition from early-time deceleration to late-time acceleration around  $z \approx 0.7$ , in excellent agreement with DESI reconstructed expansion history. These correspondences validate the physical viability of the  $f(\mathbb{Q}, \mathbb{T})$  gravity model and confirm that the geometrically induced cosmic evolution is not only mathematically consistent but also in strong agreement with the most recent cosmological observations.

## Appendix A: Calculation of $\omega'_{DE}$

$$\begin{aligned}
\omega'_{DE} = & \left[ 2^{-\frac{3m}{8}-u-\frac{7}{2}} 3^{-\frac{3m}{8}-u-\frac{5}{2}} m^{-u} \left( \frac{H_0^2 \Upsilon^{2q+2}}{m^2} \right)^{-\frac{3m}{8}} \left\{ -2^{\frac{3m}{8}+u+\frac{7}{2}} 3^{\frac{3m}{8}+u+\frac{3}{2}} \right. \right. \\
& \times (3m+4) (H_0^2 \Upsilon^{2q+2})^{u+\frac{3}{2}} \left\{ 12H_0^2 \Upsilon^{2q+2} - 12H_0^2 (u+1) \Upsilon^{2q+2} + 4H_0 (u+1) \right. \\
& \times \Upsilon^{2q+2} \left. \right\} g_1 \left( \frac{H_0^2 \Upsilon^{2q+2}}{m^2} \right)^{\frac{3m}{8}} - 2^{\frac{3m}{8}+u+\frac{5}{2}} 3^{\frac{3m}{8}+u+\frac{1}{2}} \left( u + \frac{3}{2} \right) (H_0^2 \Upsilon^{2q+2})^{u+\frac{1}{2}} \\
& \times (3m+4) \left( -4H_0 u (u+1) \Upsilon^{q+1} + 36H_0^4 \Upsilon^{4q+4} - 72H_0^4 (u+1) \Upsilon^{4q+4} \right. \\
& + 24H_0^3 (u+1) \Upsilon^{4q+4} \left. \right) g_1 \left( \frac{H_0^2 \Upsilon^{2q+2}}{m^2} \right)^{\frac{3m}{8}} - \left[ 2^{\frac{3m}{8}+u-\frac{1}{2}} 3^{\frac{3m}{8}+u+\frac{3}{2}} (3m+4) \right. \\
& \times \left( H_0^2 \Upsilon^{2q+2} \right)^{u+\frac{3}{2}} \left( \frac{H_0^2 \Upsilon^{2q+2}}{m^2} \right)^{\frac{3m}{8}-1} \left\{ -4H_0 u (u+1) \Upsilon^{q+1} + 36H_0^4 \Upsilon^{4q+4} \right. \\
& - 72H_0^4 (u+1) \Upsilon^{4q+4} + 24H_0^3 (u+1) \Upsilon^{4q+4} \left. \right\} g_1 \left. \right] \left[ m \right]^{-1} + \left[ 2^{u-\frac{3}{2}} 3^{u-\frac{1}{2}} m^u \right. \\
& \times (2u+1) \left\{ 6^{\frac{3m}{8}+2} \left\{ -2b - B_2 - B_1 \sqrt{-H_0 \Upsilon^{2q+2}} \right\} H_0^4 (3m+4) \Upsilon^{4q+4} \right. \\
& \times \left( \frac{H_0^2 \Upsilon^{2q+2}}{m^2} \right)^{\frac{3m}{8}} - 6^{\frac{3m}{8}+\frac{1}{2}} (3m+4) \sqrt{H_0^2 \Upsilon^{2q+2}} (H_0 \Upsilon^{q+1} + 6H_0^2 (6H_0^2 \Upsilon^{2q+2} \\
& + 2H_0 \Upsilon^{2q+2}) \Upsilon^{2q+2} - 36H_0^4 \Upsilon^{4q+4}) g_2 \left( \frac{H_0^2 \Upsilon^{2q+2}}{m^2} \right)^{\frac{3m}{8}} + 6^{\frac{3m}{8}} a \sqrt{\rho_0} (3H_0 m \\
& \times (3m+8) \Upsilon^{q+1} - 48H_0^2 (12H_0^2 \Upsilon^{2q+2} - 3H_0 m \Upsilon^{2q+2}) \Upsilon^{2q+2} - 432H_0^4 \\
& \times m \Upsilon^{4q+4}) \left. \right\} \left[ \sqrt{H_0^2 \Upsilon^{2q+2}} \right]^{-1} + 6^{u+\frac{1}{2}} m^u (2u+1) \sqrt{H_0^2 \Upsilon^{2q+2}} \left\{ 2^{\frac{3m}{8}+2} 3^{\frac{3m}{8}+1} \right. \\
& \times \left\{ -2b - B_2 - B_1 \sqrt{-H_0 \Upsilon^{2q+2}} \right\} H_0^2 (3m+4) \Upsilon^{2q+2} \left( \frac{H_0^2 \Upsilon^{2q+2}}{m^2} \right)^{\frac{3m}{8}} \\
& - 6^{\frac{3m}{8}+\frac{1}{2}} (3m+4) \sqrt{H_0^2 \Upsilon^{2q+2}} \left( 6H_0^2 \Upsilon^{2q+2} + 2H_0 \Upsilon^{2q+2} \right) g_2 \left( \frac{H_0^2 \Upsilon^{2q+2}}{m^2} \right)^{\frac{3m}{8}} \\
& \left. + \left[ 2^{\frac{3m}{8}-2} 3^{\frac{3m}{8}+2} \left( -2b - B_2 - B_1 \sqrt{-H_0 \Upsilon^{2q+2}} \right) H_0^4 (3m+4) \Upsilon^{4q+4} \right. \right.
\end{aligned}$$

$$\begin{aligned}
& \times \left\{ \frac{H_0^2 \Upsilon^{2q+2}}{m^2} \right\}^{\frac{3m}{8}-1} \left[ m \right]^{-1} + 6^{\frac{3m}{8}} a \sqrt{\rho_0} \left\{ -96 H_0^2 \Upsilon^{2q+2} - 72 H_0^2 m \Upsilon^{2q+2} \right. \\
& - 8(12 H_0^2 \Upsilon^{2q+2} - 3 H_0 m \Upsilon^{2q+2}) \left. \right\} - \left[ 2^{\frac{3m}{8}-\frac{3}{2}} 3^{\frac{3m}{8}-\frac{1}{2}} (3m+4) \left( \frac{H_0^2 \Upsilon^{2q+2}}{m^2} \right)^{\frac{3m}{8}} \right. \\
& \times (H_0 \Upsilon^{q+1} + 6 H_0^2 (6 H_0^2 \Upsilon^{2q+2} + 2 H_0 \Upsilon^{2q+2}) \Upsilon^{2q+2} - 36 H_0^4 \Upsilon^{4q+4}) g_2 \left. \right] \\
& \times \left[ \sqrt{H_0^2 \Upsilon^{2q+2}} \right]^{-1} - \left[ 2^{\frac{3m}{8}-\frac{7}{2}} 3^{\frac{3m}{8}+\frac{1}{2}} (3m+4) \sqrt{H_0^2 \Upsilon^{2q+2}} \left( \frac{H_0^2 \Upsilon^{2q+2}}{m^2} \right)^{\frac{3m}{8}-1} \right. \\
& \times \left\{ H_0 \Upsilon^{q+1} + 6 H_0^2 (6 H_0^2 \Upsilon^{2q+2} + 2 H_0 \Upsilon^{2q+2}) \Upsilon^{2q+2} - 36 H_0^4 \Upsilon^{4q+4} \right\} g_2 \left. \right] \\
& \times \left[ m \right] \left. \right\} \left[ (3m+4)(2u+1) (H_0^2 \Upsilon^{2q+2})^{5/2} \left\{ \rho_0 + \frac{1}{2} \left( 4a \sqrt{\rho_0} \left( \frac{H_0^2 \Upsilon^{2q+2}}{m^2} \right)^{-\frac{3m}{8}} \right. \right. \right. \\
& + 3b + B_2 + 2b \rho_0 + \sqrt{a \rho_0} (2\rho_0 + 1) - 24m^{-u} (H_0^2 \Upsilon^{2q+2})^{u+1} g_1 \\
& + B_1 \sqrt{-H_0 \Upsilon^{2q+2}} \left. \right\} \left. \right]^{-1} - \left[ 2^{-\frac{3m}{8}-u-\frac{15}{2}} 3^{-\frac{3m}{8}-u-\frac{5}{2}} m^{-u-1} \left( \frac{H_0^2 \Upsilon^{2q+2}}{m^2} \right)^{-\frac{3m}{8}-1} \right. \\
& \times (6^{u+\frac{1}{2}} m^u (2u+1) \sqrt{H_0^2 \Upsilon^{2q+2}} (6^{\frac{3m}{8}+2} \left\{ -2b - B_2 - B_1 \sqrt{-H_0 \Upsilon^{2q+2}} \right\} \\
& \times H_0^4 (3m+4) \Upsilon^{4q+4} \left( \frac{H_0^2 \Upsilon^{2q+2}}{m^2} \right)^{\frac{3m}{8}} - 6^{\frac{3m}{8}+\frac{1}{2}} (3m+4) \sqrt{H_0^2 \Upsilon^{2q+2}} \left( H_0 \Upsilon^{q+1} \right. \\
& + 6 H_0^2 (6 H_0^2 \Upsilon^{2q+2} + 2 H_0 \Upsilon^{2q+2}) \Upsilon^{2q+2} - 36 H_0^4 \Upsilon^{4q+4}) g_2 \left( \frac{H_0^2 \Upsilon^{2q+2}}{m^2} \right)^{\frac{3m}{8}} \\
& + 6^{\frac{3m}{8}} \sqrt{\rho_0} (3 H_0 m (3m+8) \Upsilon^{q+1} - 48 H_0^2 (12 H_0^2 \Upsilon^{2q+2} - 3 H_0 m \Upsilon^{2q+2}) \Upsilon^{2q+2} \\
& - 432 H_0^4 m \Upsilon^{4q+4}) \left. \right) - 2^{\frac{3m}{8}+u+\frac{7}{2}} 3^{\frac{3m}{8}+u+\frac{3}{2}} (3m+4) (H_0^2 \Upsilon^{2q+2})^{u+\frac{3}{2}} \left( \frac{H_0^2 \Upsilon^{2q+2}}{m^2} \right)^{\frac{3m}{8}} \\
& \times (-4 H_0 u (u+1) \Upsilon^{q+1} + 36 H_0^4 \Upsilon^{4q+4} - 72 H_0^4 (u+1) \Upsilon^{4q+4} + 24 H_0^3 (u+1) \\
& \times \Upsilon^{4q+4}) g_1 \left. \right] \left[ (3m+4)(2u+1) (H_0^2 \Upsilon^{2q+2})^{5/2} \left( \rho_0 + \frac{1}{2} \left( 4a \sqrt{\rho_0} \left( \frac{H_0^2 \Upsilon^{2q+2}}{m^2} \right)^{-\frac{3m}{8}} \right. \right. \right. \\
& + 3b + B_2 + 2b + \sqrt{\rho_0} (2+1) - 24m^{-u} (H_0^2 \Upsilon^{2q+2})^{u+1} g_1
\end{aligned}$$

$$\begin{aligned}
& + B_1 \sqrt{-H_0 \Upsilon^{2q+2}} \Big) \Big]^{-1} - \left[ 5 \, 2^{-\frac{3m}{8}-u-\frac{11}{2}} 3^{-\frac{3m}{8}-u-\frac{7}{2}} m^{-u} \left( \frac{H_0^2 \Upsilon^{2q+2}}{m^2} \right)^{-\frac{3m}{8}} \right. \\
& \times (6^{u+\frac{1}{2}} m^u (2u+1) \sqrt{H_0^2 \Upsilon^{2q+2}} \left( 6^{\frac{3m}{8}+2} \left\{ -2b - B_2 - B_1 \sqrt{-H_0 \Upsilon^{2q+2}} \right\} \right. \\
& \times H_0^4 (3m+4) \Upsilon^{4q+4} \left( \frac{H_0^2 \Upsilon^{2q+2}}{m^2} \right)^{\frac{3m}{8}} - 6^{\frac{3m}{8}+\frac{1}{2}} (3m+4) \sqrt{H_0^2 \Upsilon^{2q+2}} (H_0 \Upsilon^{q+1} \\
& + 6H_0^2 (6H_0^2 \Upsilon^{2q+2} + 2H_0 \Upsilon^{2q+2}) \Upsilon^{2q+2} - 36H_0^4 \Upsilon^{4q+4}) g_2 \left( \frac{H_0^2 \Upsilon^{2q+2}}{m^2} \right)^{\frac{3m}{8}} \\
& + 6^{\frac{3m}{8}} \sqrt{\rho_0} \left\{ 3H_0 m (3m+8) \Upsilon^{q+1} - 48H_0^2 (12H_0^2 \Upsilon^{2q+2} - 3H_0 m \Upsilon^{2q+2}) \Upsilon^{2q+2} \right. \\
& \left. \left. - 432H_0^4 m \Upsilon^{4q+4} \right\} \right) - 2^{\frac{3m}{8}+u+\frac{7}{2}} 3^{\frac{3m}{8}+u+\frac{3}{2}} (3m+4) \left( H_0^2 \Upsilon^{2q+2} \right)^{u+\frac{3}{2}} \\
& \times \left( \frac{H_0^2 \Upsilon^{2q+2}}{m^2} \right)^{\frac{3m}{8}} \left( -4H_0 u (u+1) \Upsilon^{q+1} + 36H_0^4 (\Upsilon+1)^{4q+4} - 72H_0^4 (u+1) \right. \\
& \times \Upsilon^{4q+4} + 24H_0^3 (u+1) \Upsilon^{4q+4} \Big) g_1 \Big) \Big] \left[ (3m+4) (2u+1) (H_0^2 \Upsilon^{2q+2})^{7/2} \left( \rho_0 \right. \right. \\
& + \frac{1}{2} \left( 4\sqrt{\rho_0} \left( \frac{H_0^2 \Upsilon^{2q+2}}{m^2} \right)^{-\frac{3m}{8}} + 3b + B_2 + 2b\rho_0 + \sqrt{\rho_0} (2\rho_0 + 1) - 24m^{-u} \right. \\
& \times (H_0^2 \Upsilon^{2q+2})^{u+1} g_1 + B_1 \sqrt{-H_0 \Upsilon^{2q+2}} \Big) \Big]^{-1} - \left[ 2^{-\frac{3m}{8}-u-\frac{9}{2}} 3^{-\frac{3m}{8}-u-\frac{5}{2}} m^{-u} \right. \\
& \times \left( \frac{H_0^2 \Upsilon^{2q+2}}{m^2} \right)^{-\frac{3m}{8}} \left\{ -\frac{\sqrt{\rho_0} \left( \frac{H_0^2 \Upsilon^{2q+2}}{m^2} \right)^{-\frac{3m}{8}-1}}{4m} - 4m^{-u} (u+1) \left( H_0^2 \Upsilon^{2q+2} \right) g_1 \right\} \\
& \times \left( 6^{u+\frac{1}{2}} m^u (2u+1) \sqrt{H_0^2 \Upsilon^{2q+2}} \left( 6^{\frac{3m}{8}+2} \left( -2b - B_2 - B_1 \sqrt{-H_0 \Upsilon^{2q+2}} \right) \right. \right. \\
& \times H_0^4 (3m+4) \Upsilon^{4q+4} \left( \frac{H_0^2 \Upsilon^{2q+2}}{m^2} \right)^{\frac{3m}{8}} - 6^{\frac{3m}{8}+\frac{1}{2}} (3m+4) \sqrt{H_0^2 \Upsilon^{2q+2}} \\
& \times (H_0 \Upsilon^{q+1} + 6H_0^2 (6H_0^2 \Upsilon^{2q+2} + 2H_0 \Upsilon^{2q+2}) \Upsilon^{2q+2} - 36H_0^4 \Upsilon^{4q+4}) \\
& \times g_2 \left( \frac{H_0^2 \Upsilon^{2q+2}}{m^2} \right)^{\frac{3m}{8}} + 6^{\frac{3m}{8}} \sqrt{\rho_0} (3H_0 m (3m+8) \Upsilon^{q+1} - 48H_0^2 (12H_0^2 \Upsilon^{2q+2} \\
& \left. \left. - 3H_0 m \Upsilon^{2q+2}) \Upsilon^{2q+2} - 432H_0^4 m \Upsilon^{4q+4} \right) \right) - 2^{\frac{3m}{8}+u+\frac{7}{2}} 3^{\frac{3m}{8}+u+\frac{3}{2}} (3m+4)
\end{aligned}$$

$$\begin{aligned}
& \times (H_0^2 \Upsilon^{2q+2})^{u+\frac{3}{2}} \left( \frac{H_0^2 \Upsilon^{2q+2}}{m^2} \right)^{\frac{3m}{8}} \left( -4H_0 u(u+1) \Upsilon^{q+1} + 36H_0^4 \Upsilon^{4q+4} \right. \\
& \left. - 72H_0^4(u+1) \Upsilon^{4q+4} + 24H_0^3(u+1) \Upsilon^{4q+4} \right) g_1 \Bigg] \left[ (2u+1) (H_0^2 \Upsilon^{2q+2})^{5/2} \left\{ \rho_0 \right. \right. \\
& \left. \left. + \frac{1}{2} \left( 4\sqrt{\rho_0} \left( \frac{H_0^2 \Upsilon^{2q+2}}{m^2} \right)^{-\frac{3m}{8}} + 3b + B_2 + 2b + \sqrt{\rho_0} (2\rho_0 + 1) - 24m^{-u} \right. \right. \right. \\
& \left. \left. \times (H_0^2 \Upsilon^{2q+2})^{u+1} g_1 + B_1 \sqrt{-H_0 \Upsilon^{2q+2}} \right\} \right]^{-1}. \tag{A1}
\end{aligned}$$

## Appendix B: Determination of $\nu_s^2$

$$\begin{aligned}
\nu_s^2 = & \left[ 2^{-\frac{3m}{8}-u-\frac{7}{2}} 3^{-\frac{3m}{8}-u-\frac{5}{2}} m^{-u} \left( \frac{H_0^2 \Upsilon^{2q+2}}{m^2} \right)^{-\frac{3m}{8}} \left( 6^{u+\frac{1}{2}} m^u (2u+1) \sqrt{H_0^2 \Upsilon^{2q+2}} \right. \right. \\
& \times \left( 6^{\frac{3m}{8}+2} \left\{ -2b - B_2 - B_1 \sqrt{\rho_0} \right\} H_0^4 (3m+4) \Upsilon^{4q+4} \left( \frac{H_0^2 \Upsilon^{2q+2}}{m^2} \right)^{\frac{3m}{8}} - 6^{\frac{3m}{8}+\frac{1}{2}} \right. \\
& \times (3m+4) \sqrt{H_0^2 \Upsilon^{2q+2}} (H_0 \Upsilon^{q+1} + 6H_0^2 (6H_0^2 \Upsilon^{2q+2} + 2H_0 \Upsilon^{2q+2}) \Upsilon^{2q+2} \\
& \left. \left. - 36H_0^4 \Upsilon^{4q+4} \right) \left( \frac{H_0^2 \Upsilon^{2q+2}}{m^2} \right)^{\frac{3m}{8}} + 6^{\frac{3m}{8}} a \sqrt{\rho_0} (3H_0 m (3m+8) \Upsilon^{q+1} - 48H_0^2 \right. \\
& \times (12H_0^2 \Upsilon^{2q+2} - 3H_0 m \Upsilon^{2q+2}) \Upsilon^{2q+2} - 432H_0^4 m \Upsilon^{4q+4} \Big) - 2^{\frac{3m}{8}+u+\frac{7}{2}} 3^{\frac{3m}{8}+u+\frac{3}{2}} \\
& \times (3m+4) (H_0^2 \Upsilon^{2q+2})^{u+\frac{3}{2}} \left( \frac{H_0^2 \Upsilon^{2q+2}}{m^2} \right)^{\frac{3m}{8}} \left( -4H_0 u(u+1) \Upsilon^{q+1} + 36H_0^4 \Upsilon^{4q+4} \right. \\
& \left. \left. - 72H_0^4(u+1) \Upsilon^{4q+4} + 24h^3(u+1) \Upsilon^{4q+4} \right) g_1 \right] \left[ 2^{-\frac{3m}{8}-u-\frac{7}{2}} 3^{-\frac{3m}{8}-u-\frac{5}{2}} m^{-u} \right. \\
& \times (H_0^2 \Upsilon^{2q+2} m^2)^{-\frac{3m}{8}} \left( -2^{\frac{3m}{8}+u+\frac{7}{2}} 3^{\frac{3m}{8}+u+\frac{3}{2}} (3m+4) (H_0^2 \Upsilon^{2q+2})^{u+\frac{3}{2}} (12H_0^2 \right. \\
& \times \Upsilon^{2q+2} - 12H_0^2(u+1) \Upsilon^{2q+2} + 4H_0(u+1) \Upsilon^{2q+2}) \left( \frac{H_0^2 \Upsilon^{2q+2}}{m^2} \right)^{\frac{3m}{8}} \\
& \left. \left. - 2^{\frac{3m}{8}+u+\frac{5}{2}} 3^{\frac{3m}{8}+u+\frac{1}{2}} (3m+4) \left( u + \frac{3}{2} \right) (H_0^2 \Upsilon^{2q+2})^{u+\frac{1}{2}} \left( -4H_0 u(u+1) \Upsilon^{q+1} \right. \right. \right. \\
& \left. \left. \times \Upsilon^{4q+4} - 72H_0^4(u+1) \Upsilon^{4q+4} + 24H_0^3(u+1) \Upsilon^{4q+4} \right) g_1 \left( \frac{H_0^2 \Upsilon^{2q+2}}{m^2} \right)^{\frac{3m}{8}} \right]
\end{aligned}$$

$$\begin{aligned}
& - \left[ 2^{\frac{3m}{8}+u-\frac{1}{2}} 3^{\frac{3m}{8}+u+\frac{3}{2}} (3m+4) (H_0^2 \Upsilon^{2q+2})^{u+\frac{3}{2}} \left( \frac{H_0^2 \Upsilon^{2q+2}}{m^2} \right)^{\frac{3m}{8}-1} \left( -4H_0 u \right. \right. \\
& + 36H_0^4 \Upsilon^{4q+4} - 72H_0^4 (u+1) \Upsilon^{4q+4} + 24H_0^3 (u+1) \Upsilon^{4q+4} \left. \right) g_1 \left. \right] \left[ m \right] \\
& + \left[ 2^{u-\frac{3}{2}} 3^{u-\frac{1}{2}} m^u (2u+1) \left( 6^{\frac{3m}{8}+2} (-2b - B_2 - B_1 \sqrt{-H_0 \Upsilon^{2q+2}} + H_0^4 \Upsilon^{4q+4} \right. \right. \\
& \times (3m+4) \left( \frac{H_0^2 \Upsilon^{2q+2}}{m^2} \right)^{\frac{3m}{8}} - 6^{\frac{3m}{8}+\frac{1}{2}} (3m+4) \sqrt{H_0^2 \Upsilon^{2q+2}} \left( H_0 \Upsilon^{q+1} \right. \\
& + 6H_0^2 (6H_0^2 \Upsilon^{2q+2} + 2H_0 \Upsilon^{2q+2}) \Upsilon^{2q+2} - 36h^4 \Upsilon^{4q+4} \left. \right) g_2 \left( \frac{H_0^2 \Upsilon^{2q+2}}{m^2} \right)^{\frac{3m}{8}} \\
& + 6^{\frac{3m}{8}} \sqrt{\rho_0} \left( 3H_0 m (3m+8) \Upsilon^{q+1} - 48H_0^2 \left( 12H_0^2 \Upsilon^{2q+2} - 3H_0 m \Upsilon^{2q+2} \right) \Upsilon^{2q+2} \right. \\
& \left. \left. - 432H_0^4 m \Upsilon^{4q+4} \right) \right] \left[ \sqrt{H_0^2 \Upsilon^{2q+2}} \right]^{-1} + 6^{u+\frac{1}{2}} m^u (2u+1) \sqrt{H_0^2 \Upsilon^{2q+2}} \left( 2^{\frac{3m}{8}+2} \right. \\
& \times 3^{\frac{3m}{8}+1} (-2b - B_2 - B_1 \sqrt{-H_0 \Upsilon^{2q+2}}) H_0^2 (3m+4) \Upsilon^{2q+2} \left( \frac{H_0^2 \Upsilon^{2q+2}}{m^2} \right)^{\frac{3m}{8}} \\
& - 6^{\frac{3m}{8}+\frac{1}{2}} (3m+4) \sqrt{H_0^2 \Upsilon^{2q+2}} \left( 6H_0^2 \Upsilon^{2q+2} + 2H_0 \Upsilon^{2q+2} \right) g_2 \left( \frac{H_0^2 \Upsilon^{2q+2}}{m^2} \right)^{\frac{3m}{8}} \\
& + 2^{\frac{3m}{8}-2} 3^{\frac{3m}{8}+2} (-2b - B_2 - B_1 \sqrt{-H_0 \Upsilon^{2q+2}}) H_0^4 (3m+4) \Upsilon^{4q+4} (H_0^2 \Upsilon^{2q+2} \\
& - 72H_0^2 m \Upsilon^{2q+2} - 8(12H_0^2 \Upsilon^{2q+2} - 3hm \Upsilon^{2q+2})) - \left[ 2^{\frac{3m}{8}-\frac{3}{2}} 3^{\frac{3m}{8}-\frac{1}{2}} \right. \\
& \times (3m+4) \left( \frac{H_0^2 \Upsilon^{2q+2}}{m^2} \right)^{\frac{3m}{8}} (H_0 \Upsilon^{q+1} + 6H_0^2 (6H_0^2 \Upsilon^{2q+2} + 2H_0 \Upsilon^{2q+2}) \Upsilon^{2q+2} \\
& - 36H_0^4 \Upsilon^{4q+4}) g_2 \left. \right] \left[ \sqrt{H_0^2 \Upsilon^{2q+2}} \right]^{-1} - \left[ 2^{\frac{3m}{8}-\frac{7}{2}} 3^{\frac{3m}{8}+\frac{1}{2}} (3m+4) \sqrt{H_0^2 \Upsilon^{2q+2}} \right. \\
& \times \left( \frac{H_0^2 \Upsilon^{2q+2}}{m^2} \right)^{\frac{3m}{8}-1} (H_0 \Upsilon^{q+1} + 6H_0^2 (6H_0^2 \Upsilon^{2q+2} + 2H_0 \Upsilon^{2q+2}) \Upsilon^{2q+2} \left. \right] \left[ m \right]^{-1} \left. \right] \\
& \times \left[ (3m+4)(2u+1) \left( H_0^2 \Upsilon^{2q+2} \right)^{5/2} \left( \rho_0 + \frac{1}{2} \left( 4\sqrt{\rho_0} \left( \frac{H_0^2 \Upsilon^{2q+2}}{m^2} \right)^{-\frac{3m}{8}} \right. \right. \right. \\
& \left. \left. + 3b + B_2 + 2b + \sqrt{\rho_0} (2\rho_0 + 1) - 24m^{-u} (H_0^2 \Upsilon^{2q+2})^{u+1} g_1 + B_1 \sqrt{-H_0 \Upsilon^{2q+2}} \right)^{-1} \right]^{-1}
\end{aligned}$$

$$\begin{aligned}
& - \left[ 2^{-\frac{3m}{8}-u-\frac{15}{2}} 3^{-\frac{3m}{8}-u-\frac{5}{2}} m^{-u-1} \left( \frac{H_0^2 \Upsilon^{2q+2}}{m^2} \right)^{-\frac{3m}{8}-1} (6^{u+\frac{1}{2}} m^u (2u+1) \sqrt{H_0^2 \Upsilon^{2q+2}} \right. \\
& \times (6^{\frac{3m}{8}+2} (-2b - B_2 - B_1 \sqrt{-H_0 \Upsilon^{2q+2}}) H_0^4 (3m+4) \Upsilon^{4q+4} \left( \frac{h^2 \Upsilon^{2q+2}}{m^2} \right)^{\frac{3m}{8}} \\
& - 6^{\frac{3m}{8}+\frac{1}{2}} (3m+4) \sqrt{H_0^2 \Upsilon^{2q+2}} (H_0 \Upsilon^{q+1} + 6H_0^2 (6H_0^2 \Upsilon^{2q+2} + 2H_0 \Upsilon^{2q+2}) \Upsilon^{2q+2} \\
& - 36H_0^4 \Upsilon^{4q+4}) g_2 \left( \frac{H_0^2 \Upsilon^{2q+2}}{m^2} \right)^{\frac{3m}{8}} + 6^{\frac{3m}{8}} a \sqrt{\rho_0} (3H_0 m (3m+8) \Upsilon^{q+1} - 48h^2 \\
& \times (12H_0^2 \Upsilon^{2q+2} - 3H_0 m \Upsilon^{2q+2}) \Upsilon^{2q+2} - 432H_0^4 m \Upsilon^{4q+4}) - 2^{\frac{3m}{8}+u+\frac{7}{2}} 3^{\frac{3m}{8}+u+\frac{3}{2}} \\
& \times (3m+4) (H_0^2 \Upsilon^{2q+2})^{u+\frac{3}{2}} \left( \frac{H_0^2 \Upsilon^{2q+2}}{m^2} \right)^{\frac{3m}{8}} (-4H_0 u (u+1) \Upsilon^{q+1} + 36H_0^4 \Upsilon^{4q+4} \\
& - 72H_0^4 (u+1) \Upsilon^{4q+4} + 24H_0^3 (u+1) \Upsilon^{4q+4}) g_1 \left. \right] \left[ (3m+4) (2u+1) (H_0^2 \Upsilon^{2q+2})^{5/2} \right. \\
& \times \left( \rho_0 + \frac{1}{2} \left( 4\sqrt{\rho_0} \left( \frac{H_0^2 \Upsilon^{2q+2}}{m^2} \right)^{-\frac{3m}{8}} + 3b + B_2 + 2b + \sqrt{\rho_0} (2+1) - 24m^{-u} \right. \right. \\
& \times (H_0^2 \Upsilon^{2q+2})^{u+1} g_1 + B_1 \sqrt{-H_0 \Upsilon^{2q+2}}) \left. \left. \right]^{-1} - \left[ 5 \cdot 2^{-\frac{3m}{8}-u-\frac{11}{2}} 3^{-\frac{3m}{8}-u-\frac{7}{2}} \right. \right. \\
& \times m^{-u} \left( \frac{H_0^2 \Upsilon^{2q+2}}{m^2} \right)^{-\frac{3m}{8}} (6^{u+\frac{1}{2}} m^u (2u+1) \sqrt{H_0^2 \Upsilon^{2q+2}} (6^{\frac{3m}{8}+2} (-2b - B_2 \\
& - B_1 \sqrt{-H_0 \Upsilon^{2q+2}}) H_0^4 (3m+4) \Upsilon^{4q+4} \left( \frac{H_0^2 \Upsilon^{2q+2}}{m^2} \right)^{\frac{3m}{8}} - 6^{\frac{3m}{8}+\frac{1}{2}} (3m+4) \\
& \times \sqrt{H_0^2 \Upsilon^{2q+2}} (H_0 \Upsilon^{q+1} + 6H_0^2 (6H_0^2 \Upsilon^{2q+2} + 2h \Upsilon^{2q+2}) \Upsilon^{2q+2} - 36H_0^4 \Upsilon^{4q+4}) g_2 \\
& \times \left( \frac{H_0^2 \Upsilon^{2q+2}}{m^2} \right)^{\frac{3m}{8}} + 6^{\frac{3m}{8}} \sqrt{\rho_0} (3H_0 m (3m+8) \Upsilon^{q+1} - 48H_0^2 (12H_0^2 \Upsilon^{2q+2} \\
& - 3H_0 m \Upsilon^{2q+2}) \Upsilon^{2q+2} - 432H_0^4 m \Upsilon^{4q+4}) \left( \frac{H_0^2 \Upsilon^{2q+2}}{m^2} \right)^{\frac{3m}{8}} - 2^{\frac{3m}{8}+u+\frac{7}{2}} 3^{\frac{3m}{8}+u+\frac{3}{2}} \\
& \times (3m+4) (H_0^2 \Upsilon^{2q+2})^{u+\frac{3}{2}} \left( \frac{H_0^2 \Upsilon^{2q+2}}{m^2} \right)^{\frac{3m}{8}} (-4H_0 u (u+1) \Upsilon^{q+1} + 36H_0^4 \Upsilon^{4q+4} \\
& - 72H_0^4 (u+1) \Upsilon^{4q+4} + 24H_0^3 (u+1) \Upsilon^{4q+4}) g_1 \left. \right] \left[ (3m+4) (2u+1) (H_0^2 \Upsilon^{2q+2})^{7/2} \right.
\end{aligned}$$

$$\begin{aligned}
& + \frac{1}{2} \left( 4\sqrt{\rho_0} \left( \frac{H_0^2 \Upsilon^{2q+2}}{m^2} \right)^{-\frac{3m}{8}} + 3b + B_2 + 2b + \sqrt{\rho_0}(2\rho_0 + 1) - (H_0^2 \Upsilon^{2q+2})^{u+1} g_1 \right. \\
& \times \left. \sqrt{-H_0 \Upsilon^{2q+2}} \right]^{-1} - \left[ 2^{-\frac{3m}{8}-u-\frac{9}{2}} 3^{-\frac{3m}{8}-u-\frac{5}{2}} m^{-u} - \left\{ \left( \frac{H_0^2 \Upsilon^{2q+2}}{m^2} \right)^{-\frac{3m}{8}-1} \right\} \right. \\
& \times \left. \{4m\} - 4m^{-u}(u+1)(H_0^2 \Upsilon^{2q+2})^u g_1 \right) (6^{u+\frac{1}{2}} m^u (2u+1) \sqrt{h^2 \Upsilon^{2q+2}} (6^{\frac{3m}{8}+2} \\
& - B_1 \sqrt{-H_0 \Upsilon^{2q+2}}) H_0^4 (3m+4) \Upsilon^{4q+4} \left( \frac{H_0^2 \Upsilon^{2q+2}}{m^2} \right)^{\frac{3m}{8}} - 6^{\frac{3m}{8}+\frac{1}{2}} (3m+4) \\
& \times \sqrt{H_0^2 \Upsilon^{2q+2}} (H_0 \Upsilon^{q+1} + 6H_0^2 (6H_0^2 \Upsilon^{2q+2} + 2H_0 \Upsilon^{2q+2}) \Upsilon^{2q+2} - 36H_0^4 \Upsilon^{4q+4}) g_2 \\
& \times \left( \frac{H_0^2 \Upsilon^{2q+2}}{m^2} \right)^{\frac{3m}{8}} + 6^{\frac{3m}{8}} \sqrt{\rho_0} (3H_0 m (3m+8) \Upsilon^{q+1} - 48H_0^2 (12H_0^2 \Upsilon^{2q+2} \\
& - 3H_0 m \Upsilon^{2q+2}) \Upsilon^{2q+2} - H_0^4 m \Upsilon^{4q+4})) - 2^{\frac{3m}{8}+u+\frac{7}{2}} 3^{\frac{3m}{8}+u+\frac{3}{2}} (3m+4) (H_0^2 \Upsilon^{2q+2})^{u+\frac{3}{2}} \\
& \times \left. \left( \frac{H_0^2 \Upsilon^{2q+2}}{m^2} \right)^{\frac{3m}{8}} (-4H_0 u(u+1) \Upsilon^{q+1} + 36H_0^4 \Upsilon^{4q+4} - 72H_0^4 (u+1) \Upsilon^{4q+4}) \right].
\end{aligned}
\tag{B1}$$

**Data Availability Statement:** No new data were generated or analyzed in support of this research.

## References

- [1] Weyl, H.: Sitzungsber. Preuss. Akad. Wiss. **465**(1918)01.
- [2] Jiménez, J.B., Heisenberg, L. and Koivisto, T.: Phys. Rev. D **98**(2018)044048.
- [3] Adak, M.: Int. J. Geom. Methods Mod. Phys. **15**(2018)1850198.
- [4] Shiravand, M., Fakhry, S. and Farhoudi, M.: Phys. Dark Univ. **37**(2022)101106; Koussour, M. et al.: Chin. J. Phys. **90**(2024)108.
- [5] Jiménez, J.B. et al.: Phys. Rev. D **101**(2020)103507.
- [6] Barros B.J. et al.: Phys. Dark Universe **30**(2020)100616.

- [7] Bajardi, F., Vernieri, D. and Capozziello, S.: Eur. Phys. J. Plus **135**(2020)912.
- [8] Sharif, M. and Ajmal, M.: Chin. J. Phys. **88**(2024)706.
- [9] Sharif, M., Gul, M.Z. and Fatima, N.: New Astron. **109**(2024)102211.
- [10] Xu, Y. et al.: Eur. Phys. J. C **79**(2019)708.
- [11] Pati, L. et al.: Eur. Phys. J. C **83**(2023)445.
- [12] Narawade, S.A., Koussour, M. and Mishra, B.: Nucl. Phys. **992**(2023)116233.
- [13] Venkatesha, V. et al.: New Astro. **105**(2024)102090.
- [14] Gadbail, G.N., Arora, S. and Sahoo, P.K.: Phys. Lett. B **838**(2023)137710.
- [15] Bourakadi, K. et al.: Phys. Dark Universe **41**(2023)101246.
- [16] Shekh, S.H. et al.: J. High Energy Astrophys. **39**(2023)53.
- [17] Gul, M.Z., Sharif, M. and Arooj, A.: Fortschr. Phys. **72**(2024)2300221; Phys. Scr. **99**(2024)045006; Gen. Relativ. Gravit. **56**(2024)45.
- [18] Khurana, M. et al.: Phys. Dark Universe **43**(2024)101408.
- [19] Pati, L. et al.: Phys. Dark Univ. **35**(2022)100925.
- [20] Agrawal, A.S., Mishra, B. and Tripathy, S.K.: J. High Energy Phys. **38**(2023)41.
- [21] Narawade, S.A., Koussour, M. and Mishra, B.: Ann. Phys. **535**(2023)2300161.
- [22] Narawade, S.A., Singh, S.P. and Mishra, B.: Phys. Dark Univ. **42**(2023)101282.
- [23] Lohakare, S.V. and Mishra, B.: Astrophys. J. **978**(2025)26.
- [24] Ratra, B. and Peebles, P.: Phys. Rev. D **37**(1988)3406; Armen-  
dariz, P.C., Mukanov, V.F. and Steinhardt, P.J.: Phys. Rev. D **63**(2001)103510.

- [25] Cai, R.G.: Phys. Lett. B **657**(2007)228; Wei, H. and Cai, R.G.: Phys. Lett. B **660**(2008)113.
- [26] Wei, H.: Class. Quantum Grav. **29**(2012)175008.
- [27] Sharif, M. and Zubair, M.: Astrophys. Space Sci. **352**(2014)263.
- [28] Jawad. A.: Eur. Phys. J. C **75**(2015)206.
- [29] Chattopadhyay, S. et al.: Astrophys. Space Sci. **353**(2014)279.
- [30] Sharif, M. and Rani, S.: J. Exp. Theor. Phys. **75**(2014)119.
- [31] Jawad, A. and Rani, S.: Adv. High Energy Phys. **2015**(2015)14.
- [32] Sharif, M. and Shah, S.A.A.: Mod. Phys. Lett. A **34**(2019)1950083.
- [33] Myrzakulov, N. et al.: J. Astron. Space Sci. **9**(2022)902552.
- [34] Dirac, P.A.M.: Proc. Math. Phys. Eng. Sci. **333**(1973)403.
- [35] Novello, M. and Bergliaffa, S.P.: Phys. Rep. **463**(2008)127.
- [36] Landau, L.D. and Lifshitz, E.M.: *The Classical Theory of Fields* (Elsevier, 2013).
- [37] Xu, Y. et al.: Eur Phys. J. C **80**(2020)22; Tayde, M. et al.: Chin. Phys. C **46**(2022)115101.
- [38] Gadibail, G.N., Mandal, S. and Sahoo, P.K.: Physics **4**(2022)1403.
- [39] Ilyas, M. and Rahman, W.U.: Eur. Phys. J. C **81**(2021)160.
- [40] Caldwell, R. and Linder, E.V.: Phys. Rev. Lett. **95**(2005)141301.
- [41] Sahni, V. et al.: Int. J. Mod. Phys. D **15**(2006)2105.
- [42] Abreu, H., Hernandez, H. and Nunez, L.A.: Class. Quantum Grav. **24**(2007)4631.
- [43] Aghanim, N. et al.: Astron. Astrophys. **641**(2020)A6.
- [44] Dunsby, P.K. and Luongo, O.: Int. J. Geom. Methods Mod. Phys. **13**(2016)1630002.
- [45] Sharif, M. and Saba, S.: Mod. Phys. Lett. A **33**(2018)1850182.